Ion-Irradiation-Assisted Phase Selection in Single Crystalline Fe_7Pd_3 Ferromagnetic Shape Memory Alloy Thin Films: From fcc to bcc along the Nishiyama-Wassermann Path

A. Arabi-Hashemi[1,*] and S. G. Mayr[1,2,3,†]

[1]*Leibniz-Institut für Oberflächenmodifizierung e.V., Permoserstraße 15, 04318 Leipzig, Germany*
[2]*Translationszentrum für Regenerative Medizin, Universität Leipzig, 04103 Leipzig, Germany*
[3]*Fakultät für Physik und Geowissenschaften, Universität Leipzig, 04103 Leipzig, Germany*

(Received 18 June 2012; published 8 November 2012)

When processing Fe-Pd ferromagnetic shape memory thin films, selection of the desired phases and their transformation temperatures constitutes one of the largest challenges from an application point of view. In the present contribution we demonstrate that irradiation with 1.8 MeV Kr^+ ions is the method of choice to achieve this goal: Single crystalline Fe_7Pd_3 thin films that are grown with molecular beam epitaxy on MgO (001) substrates and subsequently irradiated with ions reveal a phase transformation along the whole phase transformation path ranging from fcc austenite to bcc martensite. While for 10^{14} ions/cm^2 a fcc-fct phase transformation is observed, increasing the fluence to 5×10^{14} ions/cm^2 and 5×10^{15} ions/cm^2 leads to a phase transformation to the bcc phase. Pole figure measurements reveal an orientation relationship for the fcc-bcc phase transformation according to Nishiyama and Wassermann.

DOI: 10.1103/PhysRevLett.109.195704 PACS numbers: 81.30.Kf, 61.66.Dk, 61.80.−x, 64.70.K−

Fe-Pd based alloys have attracted tremendous interest during the past 30 years—initially due to their Invar [1] as well as magnetic properties [2], and, more recently, owing to their magnetic shape memory (MSM) behavior [3] with theoretical strains up to approximately 5%. Their main advantages over the most common MSM alloy, Ni-Mn-Ga, are higher ductility and recently demonstrated biocompatibility [4]; applications such as biomedical actuators or sensors thus seem possible. Fe_7Pd_3 exhibits four different metastable phases: the austenite fcc phase and three martensite phases (fct, bct, and bcc) [5]. The MSM effect due to variant reorientation is only observed within the fct phase, since only this phase fulfills both the requirements of a high mobility of twinning dislocations and a high magnetocrystalline anisotropy [6]. The metastable phase diagrams for bulk poly- and single crystals [5,7,8] reveal that to obtain the fct phase at room temperature the composition must be controllable by a few 0.1 at.%, while thin film stresses due to substrate constraints [9] and surfaces [10] shift phase equilibria—similar to external stresses [11]. Inspired by these effects, the present work aims at exploring the influence of generalized internal stresses due to (i) point defects and (ii) deviations from equilibrium short-range order. While the former are stresses in a strict mechanical sense, the latter are defined here as the conjugate variable of the short-range order parameter. The presence of short-range order in relaxed Fe-Pd samples has, in fact, been demonstrated in recent conversion electron Mößbauer spectroscopy measurements [12]. In a given sample, manipulation of both, (i) and (ii) can conveniently be achieved by means of irradiation with energetic ions (see, e.g., Ref. [13] for a suitable review on ion-induced effects in matter).

Crystallography of the martensite transformation in Fe_7Pd_3 is far from being understood in all its details at this point: While the twinning mechanism for the fcc ↔ fct transformation has been studied [14] and the habit plane has been predicted on theoretical grounds [15], it has never been observed experimentally. The orientation relationship (OR) between parent and product phases, on the other hand, has neither been clarified theoretically nor experimentally. A precise knowledge of the latter is essential for the understanding of all phenomena related to the martensite phase—including magnetically induced reorientation of martensite variants, viz. the MSM effect. Since the OR is unknown at this point, many authors (e.g., Ref. [9]) assume a Bain [16] OR. Although the latter can be formally employed for transforming the phases into one another (and thus for thermodynamic integration [10]), it has to be regarded as approximation and has never been observed experimentally. In fact, pure Bain transformation resulting in a Bain OR can never leave one plane undistorted and unrotated. The existence of this so-called habit plane is, however, the basic principle of the phenomenological theories of Wechsler, Lieberman, and Read [17] and Bowles and MacKenzie [18]. According to these theories, a fcc-bcc martensite transformation can be described by a Bain strain, a rigid body rotation and a lattice invariant deformation, which can be twinning or slip. Thus the study of the OR between parent and product phase is essential to understand the crystallography of the martensite transformation. Experimentally observed OR are generally given by Kurdjumov and Sachs [19], Nishiyama and Wassermann (NW) [20,21], Pitch [22], and Greninger and Troiano [23].

500 nm thick Fe_7Pd_3 films were epitaxially deposited with total deposition rates of 1.5 Å/s on MgO (001) single crystalline substrates with epipolished surfaces [24]. Films were synthesized at 850 °C by two independently rate controlled electron beam evaporators in a UHV system

with a base pressure better than 3×10^{-9} mbar. To exclude errors due to compositional fluctuations, each of the 1 cm^2 large samples were cut into four pieces, three of which were irradiated with 1.8 MeV Kr^+ ions up to different fluences—10^{14} ions/cm^2, 5×10^{14} ions/cm^2, and 5×10^{15} ions/cm^2 for the sample presented in the following. The composition measured by EDX was Fe-29 at.% Pd, which means that the sample resides very close to the phase transformation fcc $\leftrightarrow$ fct [7,8]. A $\theta - 2\theta$ XRD measurement revealed the prevalent austenite (fcc) phase of the unirradiated sample with a lattice parameter of (3.77 ± 0.01) Å.

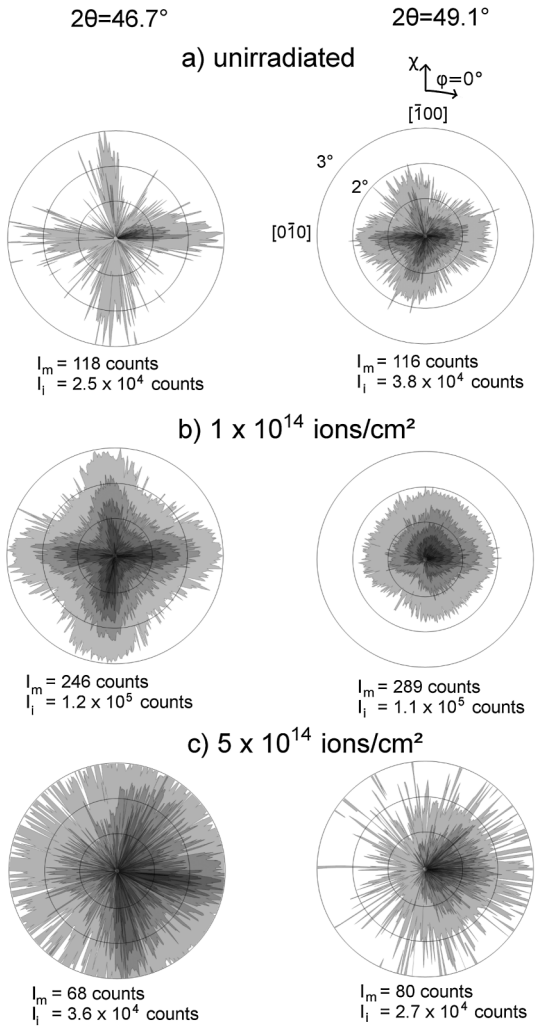

FIG. 1. Stereographic projections onto the austenite fcc (001) plane of the (200)/(020) and (002) fct pole figure measurements. While χ ranges from 0° to $\chi = 3°$, the circles have a step increment of 1°. Pole figures in the left and right columns are measured at $2\theta = 46.7°$ (long axis perpendicular to surface) and $2\theta = 49.1°$ (short axis perpendicular to surface), respectively. Also given are the maximum (I_m) and integrated (I_i) intensities. The measurements reveal a fcc to fct phase transformation for a fluence of 10^{14} ions/cm^2. A fluence of 5×10^{14} ions/cm^2 results in transformation towards the bcc phase.

Three pole figures were measured for each fluence: Two were conducted for the fct phase at $2\theta = 46.7°$ and $2\theta = 49.1°$, corresponding to variants with their long a and short c axes, respectively, aligned normal to the surface or, equivalently, the (200)/(020) and (002) reflexes of fct. Pole figures were generally recorded from $\varphi = 0°$ to $\varphi = 360°$, while for the fct pole figures $\chi = 0°$ to $\chi = 3°$ was chosen. Here, χ denotes the tilt angle and φ the angle of rotation, as shown in Fig. 1. This χ range covers all poles of the fct variants, since the tilt angle for a fct variant is less than 1.6° [25]. The bcc phase was investigated by one pole figure in the range from $\chi = 0°$ to $\chi = 88°$ and at an angle of $2\theta = 62.3°$, where diffraction from {200} planes can be observed. The angular increment of the measurements was chosen as 1° for χ and φ, while the integration time for each data point was 1.0 sec for fct and 0.6 sec for bcc pole figures. The whole set of parameters is summarized in Table I.

The fct pole figures are shown in Fig. 1, as measured at $2\theta = 46.7°$ (left) and $2\theta = 49.1°$ (right), respectively. For the unirradiated film only weak intensities of 118 and 116 counts are detected for both of its fct pole figures, while the integrated intensities yield 2.5×10^4 and 3.8×10^4 counts for the fct poles at $2\theta = 46.7°$ and $2\theta = 49.1°$, respectively. The existence of minor amounts of fct martensite in the unirradiated film clearly reflects the proximity to the austenite $\leftrightarrow$ martensite phase transformation. Irradiation with 10^{14} ions/cm^2 creates a more distinct fourfold pattern for both fct pole figures and leads to an increase of maximum intensities to 246 ($2\theta = 46.7°$) and 289 counts ($2\theta = 49.1°$). The integrated intensities increase to 1.2×10^5 ($2\theta = 46.7°$) and 1.1×10^5 ($2\theta = 49.1°$) counts, which correspond to a relative increase of fct contributions by factors of 4.8 ($2\theta = 46.7°$) and 2.9 ($2\theta = 49.1°$). The fct pole figures show an alignment of the tilted cells along [100] and [010], as can be seen in Fig. 1(b). This finding is in accordance with the fcc-fct transformation mechanism of Refs. [14,26], that propose shear along $\{110\}_a\langle 1\bar{1}0\rangle_a$, where the subindex represents the austenite phase. A higher fluence of 5×10^{14} ions/cm^2 leads to decreasing maximum (68 and 80 counts) and integrated (3.6×10^4 and 2.7×10^4 counts) intensities for

TABLE I. Parameters underlying the present pole figure measurements: fct and bcc pole figures where measured from $\chi = 0°$ to $\chi = 3°$ and $\chi = 0°$ to $\chi = 88°$, respectively. For the sake of completeness the experimentally observed fcc lattice parameter is also given.

Phase	Lattice parameter [Å]	2θ[°]	Measured χ-range [°]
fcc	$a_0 = 3.77$	...	...
fct	$a = 3.89$	46.7	0–3
	$c = 3.71$	49.1	0–3
bcc	$a_0' = 2.98$	62.3	0–88

the fct phase, indicating further transformation towards bcc. The fct pole figures of the 5×10^{15} ions/cm^2-irradiated sample is not shown in Fig. 1, since its shape, maximum intensities of 64 and 84 counts and integrated intensities of 2.4×10^4 and 2.0×10^4 counts are very close to the data obtained for 5×10^{14} ions/cm^2.

At $2\theta = 62.3°$, diffraction from {200} planes of the bcc phase of Fe_7Pd_3 can be observed. Prior to ion irradiation, the $2\theta = 62.3°$ pole figure exhibits four peaks, that can be assigned to MgO {220} diffraction. This can also be found at $2\theta = 62.3°$—keeping in mind that all measurements within this manuscript were performed with the MgO substrate attached. As shown in Fig. 2(a), irradiation with 10^{14} ions/cm^2 does not induce additional poles in the bcc pole figure, because this fluence results in a fcc-fct phase transformation, as explained before. Irradiation with 5×10^{14} ions/cm^2 leads to the appearance of four new poles at $\chi \approx 8°$ and twelve new poles at $\chi \approx 45°$, as depicted in Fig. 2(b). Four of the new {200} bcc poles overlap with the {220} diffraction peaks of the MgO substrate, which can both be found at $\chi = 45°$ and $\varphi = 0°$, 90°, 180°, and 270°. This overlapping can be uncovered by exactly comparing these four peaks in Fig. 2(b) with 2(a). When irradiating the sample with 5×10^{14} ions/cm^2, a broadening of the latter can be observed. This indicates the existence of four new {200} bcc poles, which can be assigned to the variants 11, 5, 10, 7, 8, 2, 4 and 1, as shown in Fig. 2(d). At each of these four poles we find two variants. When comparing the fct and bcc pole figures of the 5×10^{14} ions/cm^2-irradiated sample with the pole figures of the 10^{14} ions/cm^2-irradiated sample [fct: Figs. 1(b) and 1(c); bcc: Figs. 2(a) and 2(b)] an increased amount of the bcc phase and a simultaneously reduced amount of fct phase can be observed. This finding nicely illustrates, that irradiation with 5×10^{14} ions/cm^2 transforms fcc to bcc with an intermediate fct phase, as expected. Irradiation with 5×10^{14} ions/cm^2 on the other

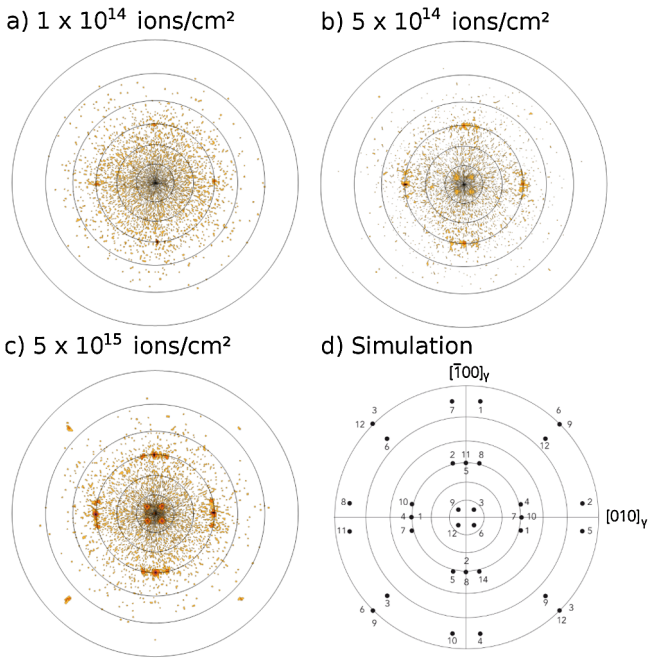

FIG. 2 (color online). Stereographic projections onto the austenite fcc (001) plane of {200} pole figure measurements at $2\theta = 62.3°$ ranging from $\chi = 0°$ to $\chi = 88°$—after 1.8 MeV Kr^+ ion irradiation with fluences of (a) 10^{14} ions/cm^2, (b) 5×10^{14} ions/cm^2 and (c) 5×10^{15} ions/cm^2. (d) shows a pole figure simulation of an OR according to NW (ranging to $\chi = 90°$). The large circles represent equidistant χ increments of 15°, while the numbers denote 12 variants.

TABLE II. Simulated and experimentally observed positions of the {200} peaks of pole figure measurements. The simulated positions are derived from the 12 martensite variants according to the NW OR transformed from a (001)[100] austenite [27]. The plane of projection is austenite fcc (001).

	Simulation		Experiment	
Variant	χ[°]	φ[°]	χ[°] ± 1°	φ[°] ± 1°
	83.1	6.9	...	...
1	45.8	103.6	43.7	102.7
	45.0	270.0	45.0	269.2
	83.1	83.1	...	...
2	45.8	346.4	44.1	347.6
	45.0	180.0	44.9	180.5
	9.7	45.0	8.2	45.8
3	80.3	225.0	80.1	225.2
	83.1	173.1	...	...
4	45.8	76.4	44.4	76.5
	45.0	270.0	45.0	269.2
	83.1	96.9	...	...
5	45.8	103.6	43.7	103.7
	45.0	0.0	44.5	1.7
	9.7	135.0	8.7	138.8
6	80.3	315.0	80.4	315.7
	83.1	353.1	...	...
7	45.8	256.4	44.9	258.6
	45.0	90.0	44.9	90.0
	83.1	286.9	...	...
8	45.8	13.6	44.0	12.9
	45.0	180.0	44.9	180.5
	9.7	315.0	8.3	311.5
9	80.3	135.0	80.4	135.9
	83.1	186.9	...	...
10	45.8	283.6	44.0	283.0
	45.0	90.0	44.9	90.0
	83.1	253.1	...	...
11	45.8	166.4	45.0	169.0
	45.0	0.0	44.5	1.7
	9.7	225.0	8.4	223.8
12	80.3	45.0	79.8	45.9

hand clearly leads to a pronounced bcc pole figure, as shown in Fig. 2(b).

Measured {200} bcc poles and their simulated counterparts, assuming an OR according to NW, show excellent agreement [Figs. 2(c) and 2(d)]. The stereographic projection of the simulated pole figure of Fig. 2(d) has been derived employing data from Ref. [27]. Table II compares {200} experimental (5×10^{15} ions/cm^2) and simulated poles due to NW. The OR according to NW is given by

$$\{111\}_a \| \{110\}_m \quad \text{and} \quad \langle 112\rangle_a \parallel \langle 110\rangle_m$$

Each bcc variant is cubic and therefore shows three {200} poles in the pole figure simulation. Four poles can be found at $\chi = 90°$. These poles belong to the variants 3, 12, 6 and 9, as can be seen in Fig. 2(d). These four poles are not measured in the {200} bcc pole figure because the range of the pole figure was $\chi = 0°$ to $\chi = 88°$. Even when extending the range of measurement to $\chi = 90°$ these poles would not be accessible without tilting the sample. Additional eight poles are missing in the bcc pole figure of Fig. 2(c), which can be found in the simulation at $\chi = 83.1°$. This might be due to reduced x-ray intensity for high χ angles. The intensities of the bcc pole figures are represented in logarithmic scale.

When comparing the shear underlying the NW OR $\{111\}_a\langle 112\rangle_a$ [28]—as observed for the fcc-bcc transformation—with transformation shear of fcc-fct given by $\{110\}_a\langle 1\bar{1}0\rangle_a$ according to Ref. [26], it can be concluded that two different shear systems are involved along the fcc-fct-bcc martensite transformation. These two shear systems might explain two frequently observed phenomena: (i) The spearhead structure within the fct matrix, which is found when transforming from fct to bct-bcc [8] is a result of intersecting shear systems; (ii) the nonthermoelasticity of the fcc-bcc martensite transformation [29] might also be caused by the intersection of both differently orientated shear systems.

The amount of the austenite fcc phase in the unirradiated sample which transforms to martensite fct and bcc due to ion irradiation is estimated by $\theta - 2\theta$ XRD measurements of the four samples. The intensity of the (200) fcc peak of the unirradiated sample falls to 5% (4%, 2%) after ion irradiation with 1×10^{14} ions/cm^2 (5×10^{14} ions/cm^2, 5×10^{15} ions/cm^2). This means that almost the whole fcc phase transforms due to ion irradiation. This finding is confirmed by SEM and AFM measurements which show surface twins covering the whole surface of the irradiated samples. Since the unirradiated sample is in the austenite phase it does not show any surface twins at all.

In the following we aim to address the physical foundations of ion-irradiation-induced phase tuning in Fe-Pd. As mentioned in the very beginning of this Letter, our present study was initially motivated by the notion that generalized stresses due to point defects and disorder within the sample are capable of increasing the austenite-martensite, as well as the intermartensite transition temperatures—just like external stresses do as described by the Clausius-Clapeyron equation [30]. It is well established [13] that 1.8 MeV Kr^+ irradiation at room temperature introduces Frenkel pairs and disorder within the sample, while also extended thermal spikes occur in the course of a collision cascade. As the latter constitutes local liquidlike regions that are rapidly cooled down within some psec by the surrounding materials, it seems necessary to separate thermal-spike related materials modification from the impact of point defects and disorder. To this end, we verified that an equivalent dose (in terms of defect generation densities) of 1.9 MeV He^+ ions is capable of inducing a similar phase change as 1.8 MeV Kr^+. Indeed, the Fe_7Pd_3 films transform from austenite to martensite at a fluence of 3.7×10^{17} ions/cm^2. As extended thermal spikes are established to be absent during He^+ irradiation, this finding strongly supports the picture that defects and disorder are the clue to develop an understanding. As recent conversion electron Mößbauer spectroscopy measurements of the present samples indicate, ion irradiation at ambient conditions only has a minor effect on short-range order or disorder in Fe-Pd [31]. Based on these findings we conclude that ion-irradiation induced point defects are the origin of the presently observed phase transition—most prominently interstitials due to their higher stress fields than vacancies.

To conclude, ion irradiation allows for fine-tuning of the austenite and martensite phases from fcc to bcc in Fe-Pd MSM alloys. Furthermore, the OR for the fcc to bcc phase transformation was determined to be according to NW. Two different shear systems are involved in the martensite transformation. While the shear system of the fcc-bcc transformation is $\{111\}_a\langle 112\rangle_a$, the shear observed for the fcc-fct transformation is $\{110\}_a\langle 1\bar{1}0\rangle_a$. Thus, the possibility of inducing the martensite transformation and fine-tuning the martensite phases by ion irradiation provides a way to sustainably manipulate the Fe_7Pd_3 phase post deposition—for use in application and further fundamental studies on the nature of the transformation.

It is a pleasure for us to thank Professor R. S. Averback (UIUC) and Dr. D. Spemann (Leipzig) for facilitating ion irradiation, Dr. J. Gerlach for discussions and Professor Dr. Dr.h.c. B. Rauschenbach for general support. We gratefully acknowledge financial support from the Leipzig Graduate School of Natural Sciences, Building with Molecules and Nano Objects (BuildMoNa) through the German Science Foundation (DFG), the European Union and the Free State of Saxony as well as the German Federal Ministry of Education and Research (BMBF, PtJ-BIO, 0315883).

*ariyan.arabi-hashemi@iom-leipzig.de
†Corresponding author.
stefan.mayr@iom-leipzig.de

[1] M. Matsui, T. Shimizu, H. Yamada, and K. Adachi, J. Magn. Magn. Mater. **15–18**, 1201 (1980).

[2] H. A. Durr, E. Dudzik, S. S. Dhesi, J. B. Goedkoop, G. van der Laan, M. Belakhovsky, C. Mocuta, A. Marty, and Y. Samson, Science **284**, 2166 (1999).
[3] R. D. James and M. Wuttig, Philos. Mag. A **77**, 1273 (1998).
[4] Y. Ma, M. Zink, and S. G. Mayr, Appl. Phys. Lett. **96**, 213703 (2010).
[5] H. M. Matsui, H. Yamada, and K. Adachi, J. Phys. Soc. Jpn. **48**, 2161 (1980).
[6] R. D. James, R. Tickle, and M. Wuttig, Mater. Sci. Eng. A **273–275**, 320 (1999).
[7] M. Sugiyama, R. Oshima, and F. E. Fujita, Trans. Jpn. Inst. Met. **25**, 585 (1984).
[8] J. Cui, T. W. Shield, and R. D. James, Acta Mater. **52**, 35 (2004).
[9] J. Buschbeck, I. Opahle, M. Richter, U. K. Rößler, P. Klaer, M. Kallmayer, H. J. Elmers, G. Jakob, L. Schultz, and S. Fähler, Phys. Rev. Lett. **103**, 216101 (2009).
[10] S. G. Mayr, Phys. Rev. B **85**, 014105 (2012).
[11] H. Kato, Y. Liang, and M. Taya, Scr. Mater. **46**, 471 (2002).
[12] I. Claussen, R. A. Brand, H. Hahn, and S. G. Mayr, Scr. Mater. **66**, 163 (2012).
[13] R. Averback and T. D. de la Rubia, in *Solid State Physics*, Displacement Damage in Irradiated Metals and Semiconductors Vol. 51, edited by H. Ehrenreich and F. Spaepen (Academic, New York, 1997), p. 281.
[14] M. Sugiyama, R. Oshima, and F. E. Fujita, Trans. Jpn. Inst. Met. **27**, 719 (1986).
[15] H. Kato, T. Wada, Y. Liang, T. Tagawa, M. Taya, and T. Mori, Mater. Sci. Eng. A **332**, 134 (2002).
[16] E. C. Bain and N. Y. Dunkirk, Trans. Am. Inst. Min., Metall. Pet. Eng. **70**, 25 (1924).
[17] M. S. Wechsler, D. S. Lieberman, and T. A. Read, Trans. Am. Inst. Min., Metall. Pet. Eng. **197**, 1503 (1953).
[18] J. S. Bowles and J. K. MacKenzie, Acta Metall. **2**, 129 (1954).
[19] G. Kurdjumov and G. Sachs, Z. Phys. **64**, 325 (1930).
[20] Z. Nishiyama, Sci. Rep. Res. Inst. Tohoku Univ., Ser. A **23**, 638 (1934).
[21] G. Wassermann, Arch. Eisenhüttenwes. **16**, 647 (1933).
[22] W. Pitch, Acta Metall. **10**, 897 (1962).
[23] A. B. Greninger and A. R. Troiano, Trans. Am. Inst. Min. Metall. Pet. Eng. **185**, 590 (1949).
[24] L. Kühnemund, T. Edler, I. Kock, M. Seibt, and S. G. Mayr, New J. Phys. **11**, 113054 (2009).
[25] Y. Ma, A. Setzer, J. W. Gerlach, F. Frost, P. Esquinazi, and S. G. Mayr, Adv. Funct. Mater. **22**, 2529 (2012).
[26] M. Foos, C. Frantz, and M. Gantois, J. Phys. IV **12**, C4 (1982).
[27] H. Kitaharaa, R. Uejib, M. Uedac, N. Tsujia, and Y. Minamino, Mater. Charact. **54**, 378 (2005).
[28] L. Sandoval, H. M. Urbassek, and P. Entel, New J. Phys. **11**, 103027 (2009).
[29] V. Sánchez-Alarcos, V. Recarte, J. Pérez-Landazábal, C. Gómez-Polo, V. Chernenko, and M. González, Eur. Phys. J. Special Topics **158**, 107 (2008).
[30] M. Kato and H.-R. Pak, Phys. Status Solidi B **123**, 415 (1984).
[31] A. Arabi-Hashemi, R. A. Brand, H. Hahn, R.S. Averback, and S. G. Mayr (unpublished).